Dynamics of large-scale brain activity in normal arousal states and epileptic seizures

P. A. Robinson,[1,2] C. J. Rennie, [1,2,3] and D. L. Rowe[1,2]

[1]*Theoretical Physics Group and Center for Wave Physics, School of Physics, University of Sydney, New South Wales 2006, Australia*
[2]*Brain Dynamics Center, Westmead Hospital and University of Sydney, Westmead, New South Wales 2145, Australia*
[3]*Department of Medical Physics, Westmead Hospital, Westmead, New South Wales 2145, Australia*

Links between electroencephalograms (EEGs) and underlying aspects of neurophysiology and anatomy are poorly understood. Here a nonlinear continuum model of large-scale brain electrical activity is used to analyze arousal states and their stability and nonlinear dynamics for physiologically realistic parameters. A simple ordered arousal sequence in a reduced parameter space is inferred and found to be consistent with experimentally determined parameters of waking states. Instabilities arise at spectral peaks of the major clinically observed EEG rhythms—mainly slow wave, delta, theta, alpha, and sleep spindle—with each instability zone lying near its most common experimental precursor arousal states in the reduced space. Theta, alpha, and spindle instabilities evolve toward low-dimensional nonlinear limit cycles that correspond closely to EEGs of petit mal seizures for theta instability, and grand mal seizures for the other types. Nonlinear stimulus-induced entrainment and seizures are also seen, EEG spectra and potentials evoked by stimuli are reproduced, and numerous other points of experimental agreement are found. Inverse modeling enables physiological parameters underlying observed EEGs to be determined by a new, noninvasive route. This model thus provides a single, powerful framework for quantitative understanding of a wide variety of brain phenomena.

I. INTRODUCTION

Correlations of electroencephalograms (EEGs) with brain function are widely used diagnostically, and close connections to dynamics and cognition are infered [1–3]. Yet the detailed link between EEGs and underlying physiology is not well understood, despite over 125 years' work [2,3]. Similar remarks apply to the evoked response potentials (ERPs) seen after impulsive stimuli, and the steady state evoked potentials (SSEPs) produced by sinusoidal stimuli [2,3]. Still more cryptic are seizure EEGs, whose relationship to normal EEGs is not understood. As a result the large array of EEG-related studies, and their highly varied results, are not integrated within any overall framework and show a divergence of approaches in which researchers working on different scales, structures, or phenomena often communicate little, and quantitative analysis usually occurs only at the smallest scales, if at all. Likewise, EEG studies are also poorly integrated with cellular neurophysiology, psychology, and other branches of neuroscience. Most information in EEGs is thus discarded because it can neither be analyzed systematically, nor in terms of physiology or other measures. Here we provide a single theory of a large variety of large-scale brain electrical activities, including seizures, establishing a framework in which other phenomena can be systematically included.

EEGs result from cortical electrical activity aggregated over scales much larger than individual neurons or than can be modeled using neural networks. Hence, models of large-scale activity average over microscopic neural structure to obtain continuum descriptions on scales of millimeters to the whole brain, incorporating realistic anatomy such as separate excitatory and inhibitory neural populations (pyramidal cells and interneurons), nonlinear neural responses, multiscale interconnections, dendritic, cell-body, and axonal dynamics, and corticothalamic feedback [4–21].

Recently we developed a physiologically based continuum model of corticothalamic dynamics that reproduced and unified many features of normal EEGs, including the discrete spectral peaks in the slow wave (<1 Hz), delta (1–2.5 Hz), theta (2.5–7.5 Hz), alpha (7.5–12.5 Hz), and beta (12.5–30 Hz) bands, seen in waking and sleeping states [13,15–20], and ERPs [21] (the upper delta boundary is lower than conventional for reasons given in [19]). Here we extend this model to account for nonlinear behaviors seen in EEGs: petit mal and grand mal generalized epilepsies, EEG entrainment and seizure activation by stimuli [2,22,23], and low-dimensional seizure dynamics [24,25]. For simplicity, we concentrate on global cases, leaving conditions such as focal epilepsies mainly for future work. In contrast to most analyses in neuroscience, which seek a specific mechanism underlying each distinct behavior, we derive a wide variety of behaviors from moderate parameter changes of a few known mechanisms in a single model. Our continuum approach averages over microstructure to yield mean-field equations in a way that is complementary to cellular-level and neural-network analyses: these other approaches can be employed to elucidate the connections between microstructure and mean-field quantities, while the continuum fields provide the background against which microscopic neural activity takes place.

After developing our model in Sec. II, our main tasks are to find parameter ranges consistent with physiology (Sec. III), understand the gross structure of the parameter space (Sec. IV), especially its division into stable and unstable zones (Sec. V), and reproduce the above experimentally observed linear (Secs. VI and VII) and nonlinear (Secs. VIII–X) behaviors in a unified way.

II. CORTICOTHALAMIC MODEL

Our focus on global dynamics allows spatial variations to be ignored. We thus use the global-mode (i.e., spatially uni-

form) limit of previous analyses [16,20] to derive ordinary differential equations for the behavior of EEG signals, generalized to include nonlinear thalamic responses. The global mode dominates at the low frequencies considered here and its use implies that boundary conditions are ignored [16,20]. We can also ignore volume conduction at the frequencies and wave numbers of relevance [19].

The mean firing rates (or *pulse densities*) Q_a of excitatory ($a=e$) and inhibitory ($a=i$) neurons are related to the cell-body potentials V_a, relative to resting, by $Q_a(t) = \Sigma[V_a(t)]$, where Σ is a sigmoidal function that increases smoothly from 0 to Q as V_a increases from $-\infty$ to ∞. We use

$$\Sigma[V_a(t)] = Q[1 + \exp\{-[V_a(t) - \theta]/\sigma'\}]^{-1}, \quad (1)$$

where θ is the mean neural firing threshold and $\sigma' \pi/\sqrt{3}$ is the standard deviation of this threshold. Effectively, the step-function threshold response of a single neuron is smeared out to yield a sigmoidal curve when averaged over the whole population.

The cell-body potential V_a results after dendritic inputs have been filtered in the dendritic tree, then summed. It obeys [15,20]

$$D_\alpha V_a(t) = \nu_{ae}\phi_e(t) + \nu_{ai}\phi_i(t) + \nu_{as}\phi_s(t - t_0/2), \quad (2)$$

$$D_\alpha = \frac{1}{\alpha\beta}\frac{d^2}{dt^2} + \left(\frac{1}{\alpha} + \frac{1}{\beta}\right)\frac{d}{dt} + 1, \quad (3)$$

where the right side of Eq. (2) involves contributions $\phi_{e,i}$ from other cortical neurons, and inputs ϕ_s from thalamic relay nuclei, delayed by a time $t_0/2$ required for signals to propagate from thalamus to cortex. Here $\nu_{ab} = N_{ab}s_b$ where N_{ab} is the mean number of synapses from neurons of type $b = e,i,s$ to type $a = e,i$ and s_b is the strength of the response to a unit signal from neurons of type b. The quantities β and α are the inverse rise and decay times of the cell-body potential produced by an impulse at a dendritic synapse, with $\beta \approx 4\alpha$ [15,18]. The second-order differential equation (2) is equivalent to the integral equation

$$V_a(t) = \int_{-\infty}^{t} L(t - t')P(t')dt', \quad (4)$$

where P is the right side of Eq. (2) and $L(t - t')$ is the response at the cell body at time t to a δ-function input to the dendrites at time t', with

$$L(u) = \frac{\alpha\beta}{\beta - \alpha}(e^{-\alpha u} - e^{-\beta u}), \quad (5)$$

which is a good approximation to the response seen experimentally.

Each part of the corticothalamic system gives rise to pulses, which form a field ϕ_a that propagates at $v = 5$–10 m s^{-1} and obeys a damped wave equation [20]. In the spatially uniform case, spatial gradient operators have no effect and the wave equation becomes
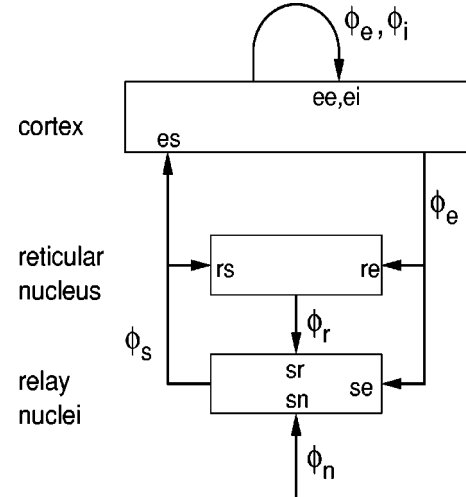

FIG. 1. Schematic of corticothalamic interactions, showing the locations ab at which ν_{ab} and G_{ab} act.

$$\left(\frac{1}{\gamma_a^2}\frac{d^2}{dt^2} + \frac{2}{\gamma_a}\frac{d}{dt} + 1\right)\phi_a(t) = \Sigma[V_a(t)], \quad (6)$$

where $\gamma_a = v/r_a$ and r_a is the mean range of axons a.

Here we make the approximation that intracortical connectivities are proportional to the numbers of synapses involved, which implies $V_i = V_e$ and $Q_i = Q_e$ [13,19] and lets us concentrate on excitatory quantities. The smallness of r_i also lets us set $\gamma_i \approx \infty$ [15].

The present model incorporates thalamic nonlinearities. Figure 1 shows the connectivities considered, including the thalamic reticular nucleus that inhibits relay nuclei. The latter relay external stimuli ϕ_n to the cortex, as well as corticothalamic feedback via projections of ϕ_e to them; their influences are excitatory. Pulse rates ϕ_r and ϕ_s in the reticular and relay nuclei, and the corresponding cell-body potentials, then satisfy

$$D_\alpha V_c(t) = \nu_{ce}\phi_e(t - t_0/2) + \nu_{cs}\phi_s(t) + \nu_{cr}\phi_r(t) + \nu_{cn}\phi_n(t), \quad (7)$$

where there is a delay $t_0/2$ for signals to travel from cortex to thalamus, $c = r,s$, $\nu_{cc} = \nu_{rn} = 0$, and the local approximation $\phi_c(t) = \Sigma[V_c(t)]$ [20] applies because the small size of the thalamic nuclei enables us to assume $\gamma_c \approx \infty$ in Eq. (6). Of the ν_{ab}, only ν_{ei} and ν_{sr} are negative. Relative to previous models, our inclusion of thalamic nonlinearity has the advantages of (i) self consistency between steady state firing rates and linear properties, which were previously determined separately, and (ii) the ability to treat widely varying values of ϕ_a, as observed in seizures.

III. PHYSIOLOGICAL PARAMETER VALUES

Our model has 15 physiological parameters: Q, θ, σ', α, β, γ_e, t_0, ν_{ee}, ν_{ei}, ν_{es}, ν_{se}, ν_{sr}, $\nu_{sn}\phi_n$, ν_{re}, and ν_{rs}. Here we use only values compatible with physiology and note that, even without this powerful constraint, only limited classes of behavior are possible given the structure of our

TABLE I. Physiologically allowed ranges and nominal values of model parameters.

Quantity	Range	Nominal	Unit
Q	100–1000	250	s^{-1}
θ	≈ 15	15	mV
σ'	≈ 3	3.3	mV
γ_e	70–150	100	s^{-1}
α	25–100	50	s^{-1}
β/α	2–6	4	
t_0	70–90	80	ms
ν_{ee}	0.05–10	1.2	mV s
$-\nu_{ei}$	0.05–10	1.8	mV s
ν_{es}	0.05–10	1.2	mV s
ν_{se}	0.05–10	1.2	mV s
$-\nu_{sr}$	0.05–10	0.8	mV s
$\nu_{sn}\phi_n$	0.05–10	1.0	mV s
ν_{re}	0.05–10	0.4	mV s
ν_{rs}	0.05–10	0.2	mV s

equations—certainly, it is not possible to fit arbitrary data. The number of parameters is big enough to allow realistic representation of the anatomy and physiology needed, but small enough to yield useful interpretations.

The first seven parameters above are approximately known from experiment, and constraints on them have been discussed elsewhere [18,19], as summarized in Table I. The ν_{ab} are less well known from physiology since the N_{ab} and s_b have only been approximately determined. Values of N_{ab} are between 100 and few thousand in the cortex and 10–100 in the thalamus [17,18], while $s_b \approx 1-100$ μV s [26]. Hence, physiology constrains the ν_{ab} only to quite broad ranges, although individual ones are better constrained than the set as a whole. We argue that all the $\nu_{ab}\phi_b$ in Eqs. (2) and (7) must be similar in size, since the anatomical structures in our model are known to affect each other comparably. Since $\phi_b \approx 5-20$ $s^{-1} \ll Q$ in normal states [27], the right sides of Eqs. (2) and (7) must be $\lesssim \theta/\phi_b$ [7]. The relative influences of the structures change significantly between states of arousal [3], which implies that changes in the $\nu_{ab}\phi_b$ must be of order σ' and the $|\nu_{ab}\phi_b|$ must typically be larger. Combining these inferences yields $\nu_{ab} \approx 0.05-10$ mV s, as in Table I. More detailed arguments to be published in the future lead to the nominal values in Table I; the latter are indicative only and are expected to vary severalfold between individuals and states of arousal.

IV. LINEAR WAVES, SPECTRA, AND EVOKED POTENTIALS

Setting all derivatives to zero in Eqs. (1)–(7) determines corticothalamic steady states when the system is driven by a constant, spatially uniform external stimulus ϕ_n. The equations are easily solved numerically and always have an odd number of solutions, usually one or three.

Small perturbations of steady states allow use of linear

analysis. In this case, a stimulus $\phi_n(\omega)$ of angular frequency ω has the transfer function to $\phi_e(\omega)$ [20,21]

$$\frac{\phi_e(\omega)}{\phi_n(\omega)} = \frac{G_{es}L}{1-G_{ei}L} \frac{G_{sn}Le^{i\omega t_0/2}}{1-S_rL^2} \frac{1}{q^2r_e^2}, \quad (8)$$

$$q^2r_e^2 = \left(1-\frac{i\omega}{\gamma_e}\right)^2 - \frac{L}{1-G_{ei}L}\left[G_{ee}+\frac{(S_d+S_iL)L}{1-S_rL^2}e^{i\omega t_0}\right], \quad (9)$$

$$G_{ab} = \frac{\phi_a(0)}{\sigma'}\left(1-\frac{\phi_a(0)}{Q}\right)\nu_{ab}, \quad (10)$$

$$L = (1-i\omega/\alpha)^{-1}(1-i\omega/\beta)^{-1}, \quad (11)$$

where the gain G_{ab} is the differential output produced by neurons a per unit input from neurons b, and the static gains for loops in Fig. 1 are $S_d = G_{es}G_{se}$ for feedback via relay nuclei only, $S_i = G_{es}G_{sr}G_{re}$ for the loop through reticular and relay nuclei, and $S_r = G_{sr}G_{rs}$ for the intrathalamic loop. Waves obey $q^2(\omega)=0$, with instability boundaries where this is satisfied for real ω [15,19].

The EEG frequency spectrum is given by the squared modulus of Eq. (8), which shows excellent agreement with observed spectra, including the occurence of alpha and beta rhythms at frequencies $f \approx 1/t_0, 2/t_0$, the asymptotic low- and high-frequency behaviors, and key differences between waking and sleep spectra [19,20]. Equation (8) also enables the form of SSEPs to be calculated, as these are the responses to sinusoidal stimuli [2]. The inverse Fourier transform of (8) gives the ERP that results from an impulse, and agrees well with experiment [21].

V. INSTABILITIES AND NONLINEAR WAVES

Since $q^2=0$ is required for instability and $|q^2|$ increases at large ω, only the first few spectral resonances can become unstable. Extensive exploration of the dynamics of the model for realistic parameter ranges implies that there are four key instabilities, which result in only a few nonlinear behaviors: (a) A slow wave/delta instability ($f \approx 0$) that leads to a low-frequency spike-wave limit cycle if only unstable fixed points remain, or to runaway to a stable high-ϕ_e fixed point that is unsustainable in practice and whose future analysis will require inclusion of effects such as hypoxia and neuro-modulator dynamics [17,18]. (This and later limit cycles are noise perturbed in practice, which may mask low level chaos, not studied here.) (b) A theta or fast delta instability, most often around 3 Hz, which saturates in a nonlinear limit cycle at nearly the same frequency [see Fig. 2(a)]. The cycle usually shows a spike-wave or polyspike form unless its parameters are close to the instability boundary. The wave form, but not its frequency, is sensitive to the input parameters. (c) A spindle instability at $\omega \approx (\alpha\beta)^{1/2}$ [see Fig. 2(b)], which is usually in the alpha band for physiological α and β,
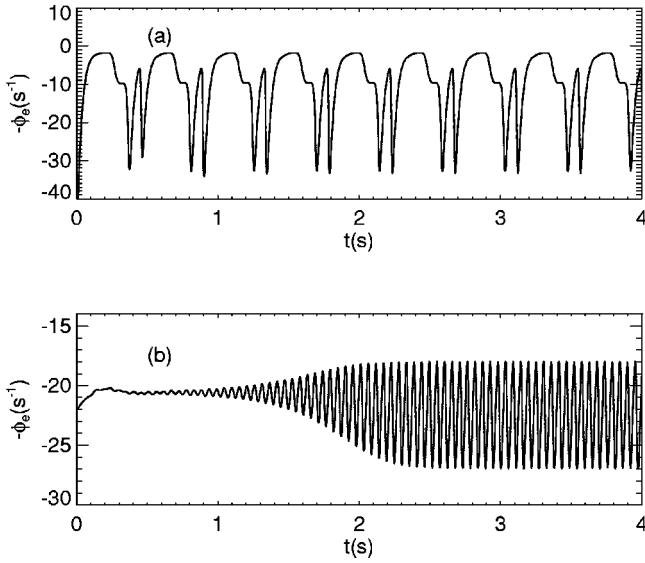
FIG. 2. Sample time series from the model in regimes corresponding to (a) theta instability, (b) spindle instability. We plot $-\phi_e$ to correspond to the customary inverted scale for scalp EEG voltages.

leading to a limit cycle near 10 Hz. This instability starts in the intrathalamic loop, then spreads to the whole system via thalamocortical projections. (d) An instability of the α peak, usually leading to a limit cycle near 10 Hz, with a wave form similar to Fig. 2(b).

The occurence of only a few important types of instability suggests that it may be possible to parameterize the stability of the brain in a space of relatively few dimensions. Indeed, at low frequencies one can write $L \approx 1$ except in the term $1 - S_r L^2$ in Eq. (9), enabling $q^2 = 0$ to be written

$$0 = \left(1 - \frac{i\omega}{\gamma_e}\right)^2 - x - \frac{y(1 - S_r)}{1 - S_r L^2} e^{i\omega t_0}, \qquad (12)$$

$$x = G_{ee}/(1 - G_{ei}), \qquad (13)$$

$$y = \frac{S_d + S_i}{(1 - S_r)(1 - G_{ei})}, \qquad (14)$$

where x and y relate to cortical and corticothalamic stability, respectively, and

$$z = -S_r \alpha\beta/(\alpha + \beta)^2, \qquad (15)$$

parametrizes intrathalamic stability. Equation (12) defines the boundary of a stability zone in xyz space, shown in Fig. 3. The signs of the gains, known from physiology, place the back of this zone at $x = 0$ and its base at $z = 0$. A pure spindle instability occurs at $z = 1$, which couples to the alpha instability, causing the upper boundaries to slope down, with spindle instability dominating at top and left, and alpha instability at right. At small z the left surface is defined by a
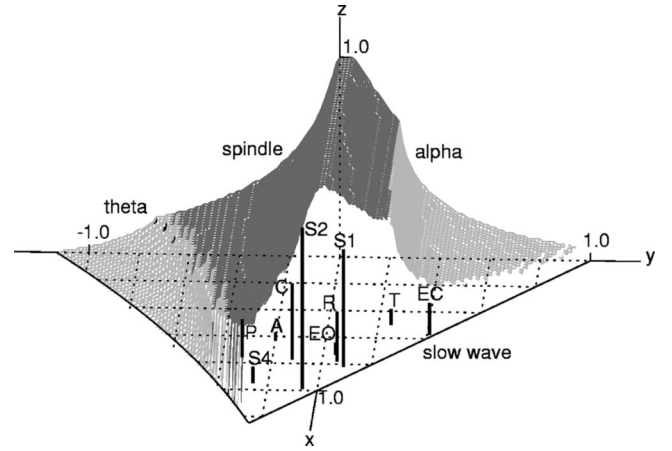

FIG. 3. Stability zone for nominal parameters in Eq. (12), except $\alpha = 60$ s^{-1}. The surface is shaded according to instability, as labeled (dark gray for spindle, light gray at right for alpha, light gray at left for theta), with the front right face left transparent as it corresponds to a zero-frequency instability. Approximate locations are shown of eyes-open (EO), eyes-closed (EC), sleep stage 1 ($S1$), $S2$, $S4$, REM (R), deep anesthesia (A), and barbiturate or alpha coma (C) states, an onset of petit mal (P), and the nominal parameters in Table I (T), with each state located at the top of its bar, whose x and y coordinates can be read from the grid. Irregularities in edges and shading are numerical artifacts. A very narrow, rapidly tapering extension of the stable zone continues to larger negative y for $x \approx z \approx 0$, but this is not shown.

theta instability, whose frequency decreases slightly toward the front. The front right surface corresponds to a zero-frequency instability and follows the plane $x + y = 1$ down to $y = y_c \approx -0.2$ where Imq^2 at small f changes sign. At $\alpha \gtrsim 100$ s^{-1} the upper boundary develops beta instability areas between the alpha and spindle areas at right, and alpha and beta areas between the spindle and theta areas. Below, we identify the boundaries with onsets of generalized seizures.

VI. STATES OF AROUSAL

Normal states must lie within the stability zone in Fig. 3. The following arguments regarding the arousal sequence, from high alertness (HA) to deep sleep, further constrain the relevant regions of parameter space and place this sequence as shown in Fig. 3: (a) Deep sleep has relatively high delta and theta amplitudes, and does not normally show alpha, except in states such as barbiturate coma. Sleep and anesthesia thus have $y \lesssim 0$, and waking the reverse. This implies $S_d + S_i < 0$ in sleep, a physiologically reasonable conclusion, since sleep is associated with increased activity in the reticular thalamic nucleus, which acts to suppress relay nuclei, attenuating incoming stimuli and positive feedback to the cortex [3]. (b) The approximately $1/f$ spectra seen at about 1–6 Hz in many subjects imply $1 - x - y \ll 1$ [19], which puts the arousal sequence near the right boundary in Fig. 3 and constrains z to be small for large $|y|$ to avoid alpha instability. (c) The large $\approx$ 10-Hz spindles seen in sleep stage 2 ($S2$) imply that this state is near the spindle instability boundary at large z, while the low-frequency content of accompanying K complexes (transient impulse responses) im-
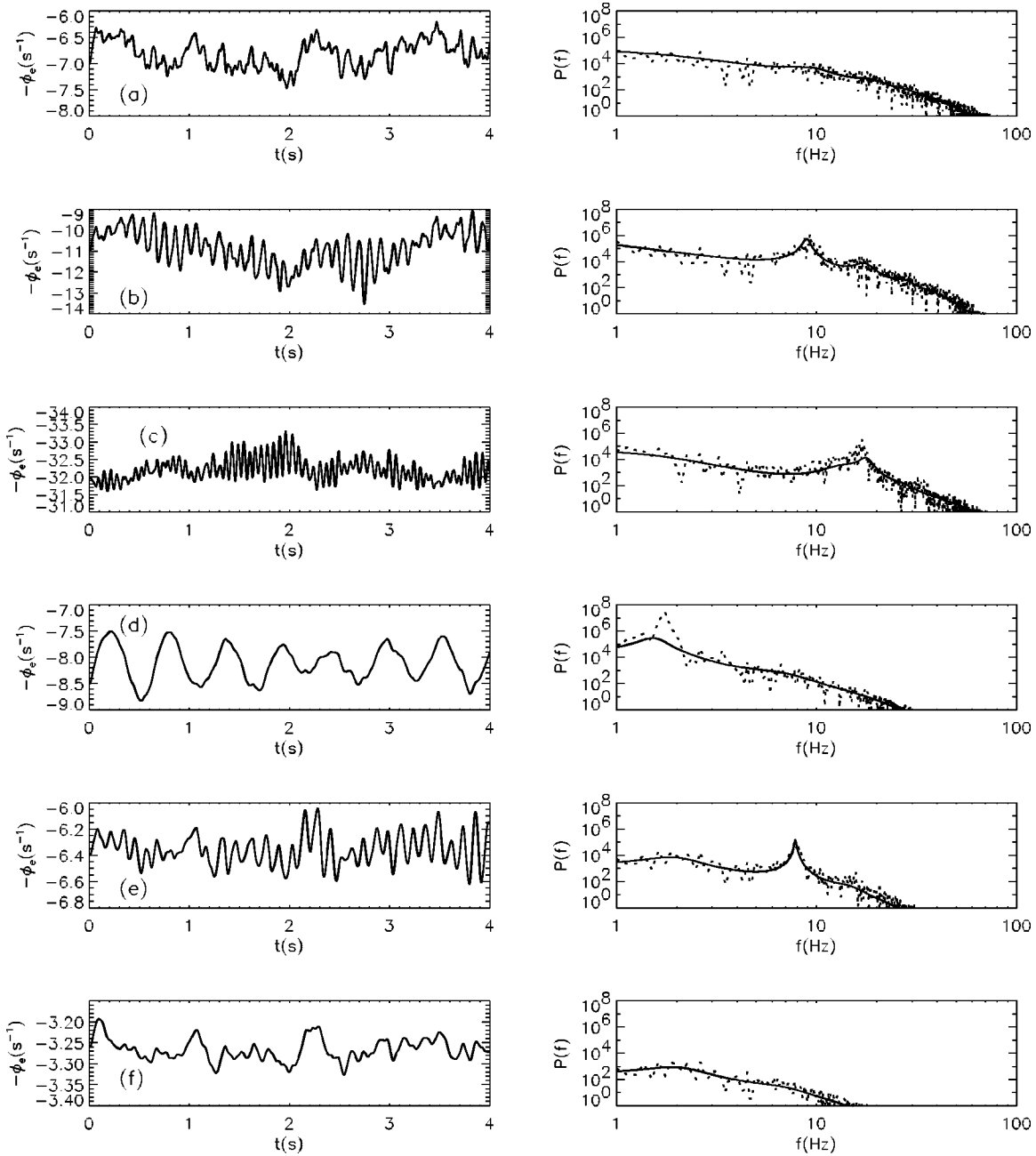
FIG. 4. Model time series (left hand frames), spectra (dotted curves in right hand frames, arbitrary units), and linear spectra from Eq. (8) (solid curves in right hand frames), for states at the points in Fig. 3 labeled (a) EO, (b) EC, (c) S2, (d) S4, (e) C, and (f) A.

plies $x \approx 1$ and $y \approx y_c$. (d) The steep low-f spectra in deep (stages 3 and 4) sleep imply $x \approx 1$ and $y \approx y_c$ [19], but with z smaller than in $S2$ because spindles are less pronounced. (e) Sharp alpha peaks in eyes-closed (EC) waking spectra put this state near the alpha boundary. (f) Weak or absent peak structure in HA, eyes-open (EO), rapid eye movement (REM) sleep, and $S1$ states [2] means they are located far from boundaries and near $y = 0$. Noting the inferred locations of other states and the fact that the arousal sequence must be continuous, REM and $S1$ must lie near $y = 0$, with HA and EO at small positive y, further from the alpha boundary than EC. A natural mechanism to decrease y at high ϕ_e exists in

that the G_{ab} increase with ϕ_a for $\phi_a < Q/2$, so the ratio of the negative feedback term (S_i, cubic in the ϕ_a) to the positive one (S_d, quadratic) grows, increasing stability. (g) Deep anesthesia is characterized by slow waves, placing it near $S4$, but its low voltage puts it further from boundaries.

Figure 4 shows model time series, spectra, and linear spectra from Eq. (8), for parameters illustrating EO, EC, $S2$, $S4$, alpha-coma, and deep-anesthesia states, holding Q, γ_e, t_0, β/α, ν_{ei}, and ν_{sn} at their nominal values, and varying α and the other ν_{ab} only moderately. The features seen in each figure strongly resemble those of the corresponding experimental data [2] and their locations in xyz space and other

properties agree with the above inferences. Moreover, sleep-state firing rates in cortical neurons, the reticular nucleus, and relay nuclei are found to be moderate, high, and low, respectively, in accord with experiment and the hypothesis that the reticular nucleus strongly affects attention by controlling the gating of incoming stimuli, while leaving the cortex active even in sleep [3,28,29].

VII. FITS TO EEG SPECTRA

To test our model and determine some of its parameters, we used a Levenberg-Marquardt method [30] to fit its linear spectrum to EEG spectra in a database collected with appropriate ethical clearances and informed consent [31]. Data were recorded at a 250-Hz sampling rate at the Cz electrode (at the top of the head) relative to a linked-ears reference using a low-pass filter with -6-dB point at 50 Hz, then processed to remove ocular artifacts [31]. For each individual and arousal state, spectra were calculated for 15 successive 8-s segments of data, averaged, then the model spectrum was fitted to this average. The relevant fit parameters were α, γ_e, t_0, G_{ee}, G_{ei}, S_d, S_i, and S_r, with $\beta/\alpha=4$ fixed. Figure 5 shows illustrative examples of the fit to the EO and EC spectra of a typical subject, demonstrating that all the major features are reproduced with reasonable accuracy.

Fits to EO and EC spectra of 103 normal adults yielded mean values of $\gamma_e=140$ s^{-1} and $t_0=85$ ms, near the nominal ones in Table I, with mean α decreasing from 103 s^{-1} to 82 s^{-1} between EO and EC. They confirm the above inferences regarding EC and EO states. Mean coordinates are $(x,y,z)\approx(0.50,0.29,0.09)$ for EC and $(0.69,0.09,0.09)$ for EO, with standard deviations of approximately $(0.03,0.02,0.01)$ in both cases. The differences in the x and y values are found to be significant at the 99.9% confidence level according to a paired-sample t-test ($p<0.001$). Full details of the experimental work, fits, and statistical tests will shortly be submitted for publication in the clinical literature, while analyses of sleep data are planned to test the model in other states of arousal.

Significantly, shifts between different states of arousal, as seen in Figs. 3 and 4, can be largely achieved by moderate changes in thalamic ν_{ab}, in accord with the central role inferred for the thalamus in determining level of attention and arousal [3,28,29].

VIII. PETIT MAL SEIZURES

Petit mal is one of the most common generalized epilepsies. Such seizures are mostly seen between ages 4 and 20, last 5–20 s, cause loss of consciousness, and show a pronounced EEG spike-wave cycle that starts and stops abruptly across the whole scalp [2]. The frequency falls gradually from around 4 Hz to under 3 Hz in most cases, and non-REM sleep and hyperventilation are powerful seizure activators. Experiments show that the loops in Fig. 1 are essential in producing petit mal, with the cortex synchronizing thalamic activity [2,10,28,32]. Also, γ-aminobutyric acid (an inhibitory neurotransmitter) antagonists such as penicillin
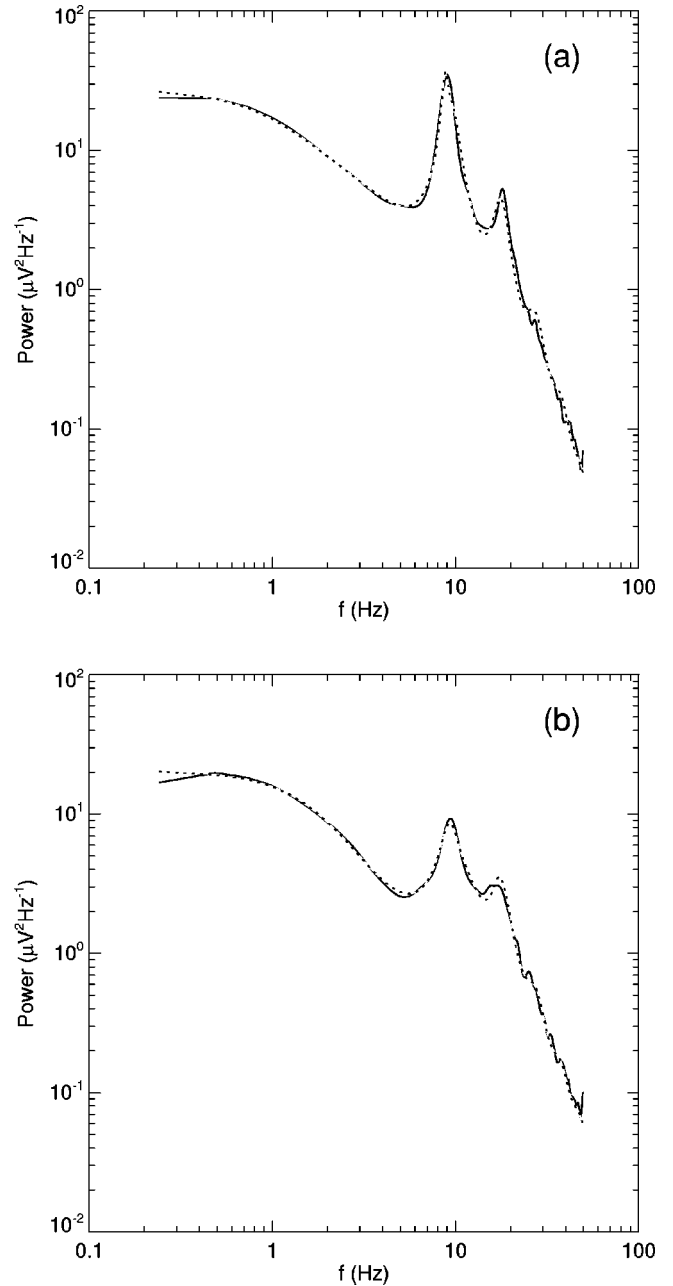

FIG. 5. Illustrative examples comparing the observed (solid curves) and fitted (dotted curves) spectra for a typical subject. (a) EC. (b) EO.

can start spike-wave oscillations, in some cases converting spindles to spike-wave complexes [2,28,32]. Similar spike-wave oscillations are seen in some partial seizures [2,25].

Our model gives rise to ≈3-Hz spike-wave cycles as the nonlinear stage of theta instability [Fig. 2(a)]. We argue that these closely resemble petit mal seizures, and the strong parameter sensitivities noted above can account for the variation seen in details of seizure wave forms [2]. The consequence that non-REM sleep must lie toward this instability boundary is consistent with Fig. 3. The role of hyperventilation is also reasonable if we assume it increases metabolic rates and, hence, the G_{ab}. This would lead toward the theta
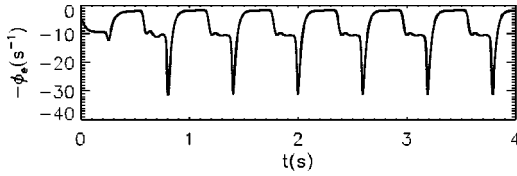
FIG. 6. Petit mal dynamics for $\alpha = 50$ s^{-1}, $t_0 = 0.2$ s, and $\gamma_e = 100$ s^{-1}. Residual flip-flop plateaus lie near $\phi_e = 2$ s^{-1} and $\phi_e = 10$ s^{-1}.

boundary due to the resulting increase in $|S_i/S_d|$, discussed above.

Analysis of the petit mal cycle in our model shows that it consists of a flip flop (a system that alternates between two states) in the limit $\gamma_e, \alpha \to \infty$, a residue of which is seen in Fig. 6, which has $t_0 = 0.2$ s for clarity. The high-ϕ_e part corresponds to large ϕ_s incident on the cortex as a result of low ϕ_r a time $t_0/2$ earlier and low ϕ_e a time t_0 earlier; the low-ϕ_e part corresponds to the converse, with near silence in relay nuclei, as seen experimentally. Signals make two circuits of the system before it returns to its original state, giving a theta-band period $2t_0$. At finite α, signals traveling via the reticular nucleus are delayed by $\approx 1/\alpha + 1/\beta$ more than those that only pass through relay nuclei. Hence, when ϕ_e flips to its upper state, there is a short period $t_0/2$ later when $S_d > |S_i|$, resulting another $t_0/2$ later in a spike of duration $\approx \alpha^{-1}$. (Polyspikes occur near the intersection of the theta and spindle instability boundaries in Fig. 3, as the result of the interplay between these two instabilities.) Finite α and γ_e also round off the other side of each square wave and finite α leads to damped ringing at $\omega = (\alpha\beta)^{1/2}$ in the intrathalamic loop. Reduction of t_0 to its physiological value restricts ringing to about one cycle before the spike. These mechanisms accord with the experimental inferences above, and observed EEGs often show a residual high-ϕ_e flip-flop plateau in each cycle [2,25,33].

Estimation of the time required to circle the dominant loop in the above mechanism implies a petit mal period

$$T \approx 2t_0 + 6/\alpha + 6/\beta + 4/\gamma_e, \tag{16}$$

which has been verified numerically, is consistent with observations, and explains the relative insensitivity of T to many parameters. The main features of the wave form, apart from spindle-related oscillations, can be found in examples with $\beta, \gamma_e = \infty$, but finite α, which implies that the three-dimensional (3D) system resulting from our equations in that limit contains the essential dynamics (a 5D system with β finite in the intrathalamic loop also reproduces spindles). This accords with recent findings that dimensions of time series of petit mal and related seizures are low [24,25,33]. If t_0 and γ_e do not change from EO values, the frequency drop during seizure then implies a decrease in α from $\gtrsim 100$ s^{-1} to $\lesssim 50$ s^{-1}, which is plausible given the change between EO and EC and the need for $\alpha = 20-40$ s^{-1} in $S2$ to account for spindles as intrathalamic resonances.

A typical onset point for a petit mal seizure is shown in Fig. 3. Transformation of spindles into petit mal is inferred to

occur by moving from the vicinity of $S2$ to the theta instability zone, with a rapid switch of activity from roughly 10 Hz to 3 Hz, as seen experimentally [32]. Large values of γ_e favor instability, which may explain the typical onset of petit mal at around age 4, since γ_e rises in children due to myelination. The typical upper limit at age 20 must be due to other parameter changes.

IX. GRAND MAL SEIZURES

After a short transient in which there is a sudden reduction in EEG amplitude, grand mal seizures display a tonic phase of large, roughly 10-Hz oscillations, lasting about 10 s. The following clonic phase lasts around 10 s, dominated by polyspike-wave complexes that fall in frequency from roughly 4 to 1 Hz. A period of very low amplitude EEG follows, slowly giving way to normal activity. Grand mal with primary generalization occurs often on waking, rarely in sleep, and never in REM sleep, but secondarily generalized seizures often occur in sleep. Many subjects with grand mal or petit mal have both, implying that the parameters must be similar. The thalamic structures in Fig. 1, especially the reticular nucleus, are strongly implicated in grand mal [2].

We argue that the tonic phase of grand mal is the nonlinear stage of the alpha or spindle instability of Fig. 3, that a beta subtype may exist for $\alpha \gtrsim 100$ s^{-1}, and speculate that the existence of these subtypes may account for some of the clinical variation in grand mal seizures. Onset at negative y would entail the observed amplitude reduction as the small-y zone was crossed from waking, onset at $y > 0$ on waking would involve a similar dropout in the reverse direction, while drug induced seizures may set in near the alpha coma point in Fig. 3. The clonic phase plausibly corresponds to parameter changes into the theta instability zone, causing a rapid shift in dominant frequency as petit-mal-like spike-wave complexes set in. We argue that this is followed by emergence into the region near A in Fig. 3, where EEGs are of very low amplitude, with subsequent reemergence to waking roughly along the normal arousal sequence.

In simulated spectra, we observe multiple strong harmonics of the fundamental instability frequency, which resemble the ones detected in partial seizures [34]. The effect of spatial variations remains to be incorporated here, so we cannot follow frequency variations in the fundamental frequency, for example. However, our analysis is adequate to capture features that do not depend strongly on boundary conditions (i.e., for which the relevant part of the cortex can be considered without reference to other parts).

The reduced 3D dynamical system of the preceding section can also reproduce grand mal-like time series (although not ones started via spindle instability, which require a 5D system), dominated by ≈ 10-Hz oscillations. High γ_e favors instability, in accord with the conclusion that low myelination precludes grand mal below the age of 6 months and the rarity of epileptic seizures in patients with demyelinating diseases as multiple sclerosis [2].

X. ENTRAINMENT AND SEIZURE ACTIVATION

Driving our system by adding a sinusoidal part to ϕ_n enables one to determine the steady state evoked potential
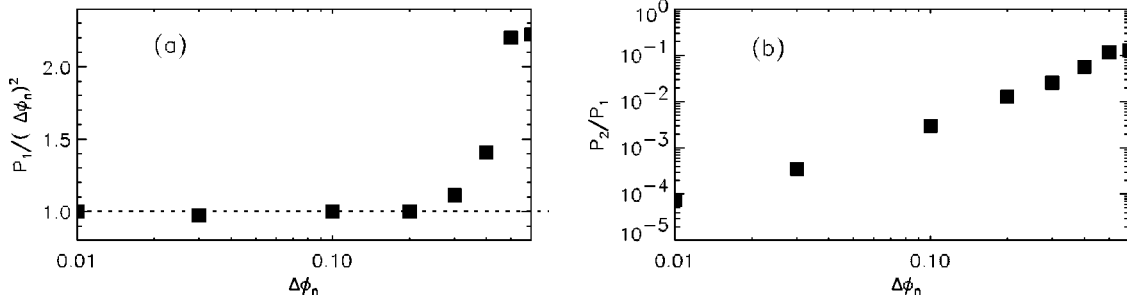
FIG. 7. Spectral densities P_1 and P_2 at the alpha resonance and its harmonic vs alpha-resonant stimulus strength $\Delta\phi_n$. (a) $P_1/(\Delta\phi_n)^2$ normalized to 1 at left. (b) P_2/P_1.

(SSEP) as a function of frequency directly. The amplitude peaks at linear resonances and is nearly proportional to that of the stimulus, except at high values where it increases rapidly and harmonics are generated (Fig. 7). This is consistent with experiments in which periodic stimuli, particularly visual, can entrain EEG activity, sharpening the alpha resonance, for example, without moving it [22], and can even lead to grand mal or petit mal seizures [2]. Significantly, the relevant resonant frequencies (5–20 Hz) span the range where photic stimulation is most effective [2].

We find similar results when noise is applied to the system, but a much higher amplitude is required to produce nonlinear effects, because the stimulus power is not concentrated at a resonant frequency. The stronger entraining effect of sinusoidally modulated light relative to periodic flashes [22], is explained by the same effect, and the global mode being the least stable [16,20] explains the stronger effect of diffuse light in inducing photic reactions [2,23], since it couples more of its power into this mode than does a localized or spatially structured source.

Recently, it was shown that $\approx 1\%$ of spontaneously occurring alpha signals show signs of nonlinearity [35–37]. This is consistent with our model, since the strongest peaks lie nearest to the alpha instability boundary, where nonlinear effects are expected to be maximal.

It is known that feedback of a subject's own EEG (e.g., via modulation of a light source) can induce seizures [38]. In our model this corresponds to introducing a positive feedback term that shifts the q^2 curve until it reaches the origin. This shift can be narrowband if bandpass-filtered EEG is fed back, leaving the remainder of the curve unaffected, and is most effective at linear resonances.

XI. DISCUSSION

The approach followed here balances the need for physiological realism against the desirability of having as few parameters as possible, leading to a model that incorporates the main features of corticothalamic physiology and anatomy using only 15 parameters. The predictions of this model provide a unified description of a wide range of phenomena, with six parameters fixed across all states, and the others only varying moderately. Of particular importance is the reduced xyz parameter space in which the stability zone of the brain is easily visualized, and arousal sequences can be con-

strained. The boundaries of this zone are identified with onsets of generalized seizures, consistent with known features of their time series and patterns of occurrence. Reduced dynamical descriptions derived from the model explain inferred low-dimensional dynamics in petit mal seizures and imply similar behavior in grand mal. Other nonlinear behaviors such as entrainment and seizure activation are also reproduced. The results support the utility of corticothalamic continuum models, while the formalism allows other loops (e.g., cortex brainstem, thalamus brainstem) to be easily included.

Fitting the model's predictions to observations provides a noninvasive probe of large-scale physiology that yields parameter values consistent with theoretical considerations and independent physiological measures. This enables states of arousal, seizure onsets, and pathologies to be assigned to distinct regions of parameter space. We find that the normal arousal sequence has a simple, ordered form in xyz space, that clinically observed waking states lie at the theoretically inferred locations, and that seizure onsets lie close to the most commonly seen precursor states. The parameter space thus provides a physiologically based organizing framework for a wide variety of phenomena. The topography of this space may in itself point the way to new connections among phenomena, such as the dual role identified here for spindle and alpha instabilities in initiating grand mal seizures. Against this topography, the significance of the parameters that distinguish the various cases, and cause transitions between them, can also be explored systematically in future work. It is hoped that the central role of relatively few parameters in this model, particularly the couplings ν_{ab}, will prompt physiologists to measure these quantities more accurately.

The above points demonstrate that the approach explored here provides a powerful framework for further studies. Spatial structure must also be included; this can be done approximately by adding $-r_a^2\nabla^2\phi_a$ to the left of Eq. (6), yielding a partial differential equation in position and time; however, in cases where part of the cortex can be treated as approximately uniform, the present analysis suffices. Equally importantly, it remains to investigate what additional factors control progression along inferred arousal sequences and into seizures or other disorders on time scales much longer than those of EEG rhythms themselves. This will require incorporation of neuromodulator dynamics [18] and brainstem reticular activation.

A key feature of our approach—and a major difference

from much of neuroscience—is that we extract a broad range of behavior from modest changes in the parameters of a single physiologically based model, without postulating extra mechanisms. Most strikingly, the distinction between seizures and normal states is simply the crossing of the relevant stability boundary, leading to a rapid change in behavior.

Thalamic couplings play central roles in determining states of arousal and attention.

[1] M.P. Stryker, Nature (London) **338**, 297 (1989).

[2] N. Niedermeyer and F. H. Lopes da Silva, *Electroencephalography: Basic Principles, Clinical Applications, and Related Fields*, 4th ed. (Williams and Wilkins, Baltimore, 1999).

[3] A.M.L. Coenen, Neurosci. Biobehav. Rev. **19**, 447 (1995).

[4] H.R. Wilson and J.D. Cowan, Kybernetik **13**, 55 (1973).

[5] F.H. Lopes da Silva, A. Hoeks, H. Smits, and L.H. Zetterberg, Kybernetik **15**, 27 (1974).

[6] P.L. Nunez, IEEE Trans. Biomed. Eng. **21**, 473 (1974).

[7] W. J. Freeman, *Mass Action in the Nervous System* (Academic, New York, 1975).

[8] F.H. Lopes da Silva, J.E. Vos, J. Mooibroek, and A. van Rotterdam, Electroencephalogr. Clin. Neurophysiol. **50**, 449 (1980).

[9] P. L. Nunez, *Electric Fields of the Brain* (Oxford, Oxford, 1981).

[10] M. Steriade, P. Gloor, R.R. Llinás, F.H. Lopes da Silva, and M.-M. Mesulam, Electroencephalogr. Clin. Neurophysiol. **76**, 481 (1990).

[11] W.J. Freeman, Int. J. Bifurcation Chaos Appl. Sci. Eng. **2**, 451 (1992).

[12] P. L. Nunez, *Neocortical Dynamics and Human EEG Rhythms* (Oxford, Oxford, 1995).

[13] J.J. Wright and D.T.J. Liley, Behav. Brain Sci. **19**, 285 (1996).

[14] V.K. Jirsa and H. Haken, Phys. Rev. Lett. **77**, 960 (1996).

[15] P.A. Robinson, C.J. Rennie, and J.J. Wright, Phys. Rev. E **56**, 826 (1997).

[16] P.A. Robinson, C.J. Rennie, J.J. Wright, and P.D. Bourke, Phys. Rev. E **58**, 3557 (1998).

[17] C.J. Rennie, P.A. Robinson, and J.J. Wright, Phys. Rev. E **59**, 3320 (1999).

[18] C.J. Rennie, J.J. Wright, and P.A. Robinson, J. Theor. Biol. **205**, 17 (2000).

[19] P.A. Robinson, C.J. Rennie, J.J. Wright, H. Bahramali, E. Gordon, and D.L. Rowe, Phys. Rev. E **63**, 021903 (2001).

[20] P.A. Robinson, P.N. Loxley, S.C. O'Connor, and C.J. Rennie, Phys. Rev. E **63**, 041909 (2001).

[21] C. J. Rennie, P. A. Robinson, and J. J. Wright, Biol. Cybernetics (to be published).

[22] R.E. Townsend, A. Lubin, and P. Naitoh, Electroencephalogr. Clin. Neurophysiol. **39**, 515 (1975).

[23] F.S.S. Leijten, E. Dekker, H. Spekreijse, D.G.A. Kasteleijn-Nolst Trenité, and W. Van Emde Boas, Electroencephalogr. Clin. Neurophysiol. **106**, 387 (1998).

[24] A. Babloyantz and A. Destexhe, Proc. Natl. Acad. Sci. U.S.A. **83**, 3513 (1986).

[25] M. Le Van Quyen, J. Martinerie, C. Adam, and F.J. Varela, Phys. Rev. E **56**, 3401 (1997).

[26] A.M. Thomson, J. Am. Math. Soc. **502**, 131 (1997).

[27] M. Steriade, I. Timofeev, and F. Grenier, J. Neurophysiol. **85**, 1969 (2001).

[28] A. Destexhe, J. Physiol. (Paris) **94**, 391 (2000).

[29] M. Steriade, Neuroscience **101**, 243 (2000).

[30] W. H. Press, B. P. Flannery, S. A. Teukolsky, and W. T. Vetterling, Numerical Recipes in C, 2nd ed. (Cambridge, Cambridge, 1992).

[31] A.R. Haig, E. Gordon, G. Rogers, and J. Anderson, Electroencephalogr. Clin. Neurophysiol. **94**, 288 (1995).

[32] G. Kostopoulos, P. Gloor, A. Pellegrini, and I. Siatitsas, Exp. Neurol. **73**, 43 (1981).

[33] M. Feucht, U. Möller, H. Witte, K. Schmidt, M. Arnold, F. Benninger, K. Steinberger, and M.H. Friedrich, Cereb. Cortex **8**, 524 (1998).

[34] S.J. Schiff, D. Colella, G.M. Jacyna, E. Hughes, J.W. Creekmore, A. Marshall, M. Bozek-Kuzmicki, G. Benke, W.D. Gaillard, J. Conry, and S.R. Weinstein, Clin. Neurophysiol. **111**, 953 (2000).

[35] C.J. Stam, J.P.M. Pijn, P. Suffczynski, and F.H. Lopes da Silva, Clin. Neurophysiol. **110**, 1801 (1999).

[36] M. Breakspear, Human Brain Mapping **15**, 175 (2002).

[37] M. Breakspear and J. Terry, Clin. Neurophysiol. (to be published).

[38] W. G. Walter, *The Living Brain* (Duckworth, London, 1953).